

The Wavelength Calibration of the WFC Grism

A. Pasquali, N. Pirzkal and J. R. Walsh

ESO/ST-ECF, Karl-Schwarzschild-Strasse 2, D-85748 Garching bei München, Germany

Abstract. We present the wavelength solution derived for the G800L grism with the Wide Field Channel from the spectra of two Galactic Wolf-Rayet stars, WR 45 and WR 96. The data were acquired in-orbit during the SMOV tests and the early INTERIM calibration program. We have obtained an average dispersion of $39.2 \text{ \AA}/\text{pix}$ in the first order, $20.5 \text{ \AA}/\text{pix}$ in the second and $-42.5 \text{ \AA}/\text{pix}$ in the negative first order. We show that the wavelength solution is strongly field-dependent, with an amplitude of the variation of about 11% from the center of the WFC aperture to the corners. The direction of the field-dependence is the diagonal from the image left top corner (amplifier A) to the bottom right corner (amplifier D). These trends are observed for all grism orders. We also describe the calibration files derived from the SMOV and INTERIM data which are used by the ST-ECF slitless extraction code aXe.

1. Introduction

The Advanced Camera for Surveys (ACS) has been designed to perform low-resolution, slitless spectroscopy over a wide range of wavelengths, from the Ly α line at $\lambda = 1216 \text{ \AA}$ to $\sim 1 \text{ \mu m}$. One *optical* grism, one *blue* prism and two *near-UV* prisms cover this range and are coupled with the Wide Field (WFC) and High Resolution (HRC) Channels, the HRC and the Solar Blind Channel (SBC) respectively.

The WFC and the HRC make use of the same grism, G800L which works between $\sim 5500 \text{ \AA}$ and $\sim 1 \text{ \mu m}$. Its nominal dispersion is $\sim 40 \text{ \AA}/\text{pix}$ and $\sim 29 \text{ \AA}/\text{pix}$ in first order for the WFC and HRC respectively.

The HRC also features a prism, PR200L, which covers the spectral range between $\sim 2000 \text{ \AA}$ and 5000 \AA , with a non linear dispersion varying from $2.6 \text{ \AA}/\text{pix}$ at $\lambda = 1600 \text{ \AA}$ to $91 \text{ \AA}/\text{pix}$ at $\lambda = 3500 \text{ \AA}$ and $515 \text{ \AA}/\text{pix}$ at $\lambda = 5000 \text{ \AA}$.

The SBC is equipped with two prisms, PR110L and PR130L which range from $\sim 1150 \text{ \AA}$ and 1250 \AA to 2000 \AA with a resolving power of ~ 80 and ~ 100 , respectively, at $\lambda = 1600 \text{ \AA}$. In particular, PR130L does not include the geocoronal L α line for low background measurements.

Pasquali et al. (2001b) showed that the high angular resolution of the ACS may easily decrease the effective resolution of the grism, since, when no slit is used, the grism nominal resolution is convolved with the object size along the dispersion axis. The extension of any grism spectrum along the cross-dispersed direction is set by the size of the object which acts as an extraction aperture. This is also an additional source of degradation when the whole spectrum is summed along the cross-dispersion axis.

The amplitude of these effects was investigated by simulating with SLIM 1.0 (Pirzkal et al. 2001b) the spectrum of the Galactic planetary nebula NGC 7009, and by increasing the linear size of the object as well as its orientation in the sky. The simulated grism spectra indicated that line blending becomes severe when objects are observed with a diameter

larger than 2 pixels ($0''.1$) and with a major axis at $PA > 45^\circ$ with respect to the dispersion axis (cf. Pasquali et al. 2001b).

These limits pose strong constraints on the selection of targets for the in-orbit wavelength calibration of the ACS spectral elements. Indeed, such calibrators have to be sorted by:

1. high brightness, to allow for short exposure times and time-series observations across the field of view;
2. a large number of emission lines in their spectra;
3. the absence of an extended nebula, which would otherwise degrade the spectral resolution;
4. negligible spectro-photometric variability, to be able to identify emission lines at any observation epoch;
5. minimum field crowding, to avoid contamination by spectra of nearby stars;
6. visibility, to allow repeated *HST* visits.

The above set of requirements rules out planetary nebulae (PNe) as possible wavelength calibrators, at least in the case of the optical G800L grism. Indeed, PNe are resolved by *HST* up to the Large Magellanic Clouds and hence do not meet requirement #3, while PNe in M31 are compact enough but faint and therefore can not fulfil requirements #1, 6 and 5 as they also lie in crowded fields (Pasquali et al. 2001a).

Wolf-Rayet stars (WRs) of spectral type WC have been shown to satisfy all the requirements, at the expense of introducing a further constraint which concerns the velocity of their stellar wind. Indeed, the wind velocity in WRs can be as slow as 700 km s^{-1} and as fast as 3300 km s^{-1} (cf. van der Hucht 2001). A typical wind speed of 2000 km s^{-1} produces a line broadening of about 1.3 and 1.9 pixels in the grism first order with the WFC and the HRC, respectively. Therefore, to limit the loss of resolution due to objects with broad emission lines, WR stars should be selected with $V_{\text{wind}} \leq 2000 \text{ km s}^{-1}$ (Pasquali et al. 2001a).

2. The Observational Strategy

We eventually selected two Galactic WR stars from the VIIth Catalogue by van der Hucht (2001) which meet the listed criteria. Their basic properties, coordinates, V magnitude and wind velocity are in Table 1.

Table 1. The WR Stars Selected for the Wavelength Calibration of the ACS Grism

Star	Spectral type	RA (2000)	DEC (2000)	V mag	Wind speed (km s^{-1})
WR 45	WC6	11:38:05.2	-62:16:01	14.80	2100
WR 96	WC9	17:36:24.2	-32:54:29	14.14	1100

Both stars had been observed from the ground with the ESO/NTT EMMI spectrograph with the purpose to acquire high-resolution spectra which would be later used as templates for the comparison with the ACS grism observations. The EMMI spectra of WR 45 and WR 96 are plotted in Figure 1, where the dispersion is 1.26 \AA/pix .

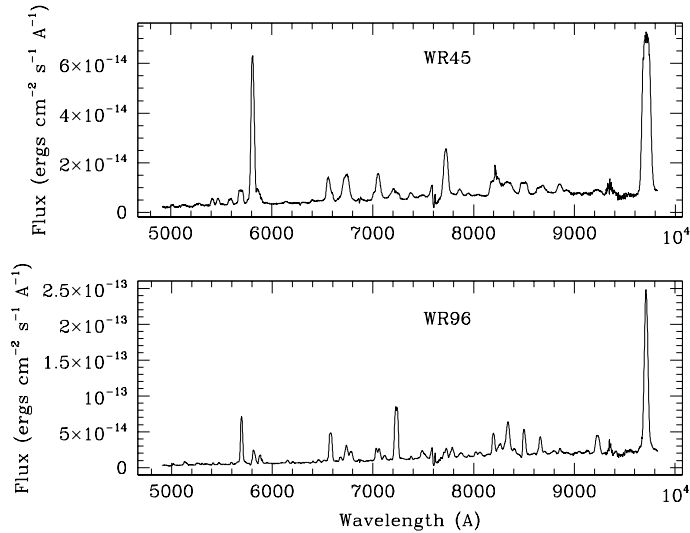


Figure 1. The spectra of WR 45 and WR 96 acquired with the ESO/NTT EMMI spectrograph with a dispersion of $1.26 \text{ \AA}/\text{pix}$.

2.1. Observations During the SMOV Tests

WR 45 was observed as part of the Servicing Mission Orbital Verification (SMOV) tests (ID 9029, PI Pasquali), at the end of April to early May 2002. Spectra were taken at five different pointings across the field of view (f.o.v) of the WFC: W1 close to the center of chip 2, W3 and W5 close to amplifiers C and D of chip 2 and W7 and W9 close to amplifiers A and B in chip 1. These pointings are shown in Figure 2.

At each position, a pair of direct and grism images were acquired, and repeated two to four times, either in the same visit or in a subsequent one to verify the stability of the filter wheel positioning. The direct image, which provides the zero point of the grism dispersion correction, was taken in the F625W and F775W filters, in order to check the target position stability with wavelength. The adopted exposure times were 1 s for the direct imaging and 20 s for the grism.

2.2. Observations During the INTERIM Program

WR 96 was observed during the INTERIM calibrations (ID 9568, PI Pasquali) in June 2002. The observational strategy was similar to WR 45, but the number of individual pointings was increased to 10 by adding to the SMOV positions the W2, W4, W8, W10 pointings and the centre of chip 1 (cf. Figure 2).

Monodimensional spectra of WR 45 and WR 96 were extracted from the raw, non drizzled images using the ST-ECF slitless spectra extraction code, aXe (Pirzkal et al. 2001a, <http://www.stecf.org/software/aXe/index.html>).

3. The Grism Characteristics

The extraction of slitless spectra relies on a number of parameters:

1. the shift in the X and Y coordinates between the position of the target in the direct image and the position of the zeroth order in the grism image;
2. the tilt of the spectra;

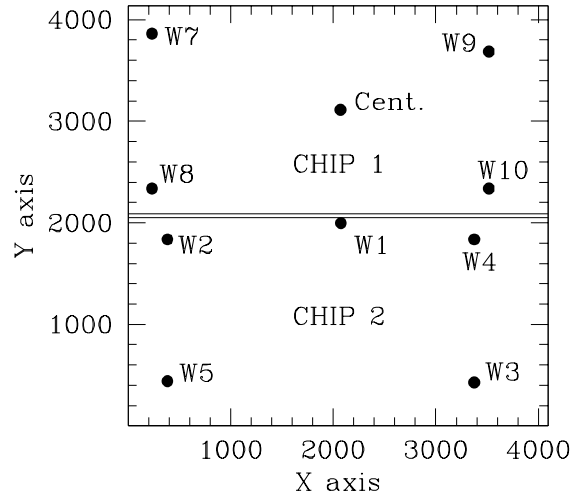


Figure 2. The pointings across the f.o.v of the WFC used during the SMOV and INTERIM observations.

3. the separation in pixels along the dispersion axis of the n th grism order from the zeroth;
4. the length in pixels along the dispersion axis of each grism order.

While the shift allows a spectrum to be identified in the grism image given the coordinates of the target in the direct image, the tilt enables it to be traced. The separation and the length of the grism orders are used to set the extraction aperture for each order spectrum.

Because of the severe geometric distortions in the WFC, these quantities are expected to be field-dependent.

3.1. The X- and Y-shifts

The X- and Y-shifts could be measured for all the pointings, except W7 and W8 whose zeroth orders fall outside the physical boundaries of the grism image. The remaining are listed in Table 2 in units of pixels; they are the difference between the target position in the direct image and the zeroth order coordinate in the grism image. The values are averages among multiple measurements available for each pointing. The standard deviation is typically 0.1 pixels.

A decrease can be recognized for the Y-shift along the diagonal from amplifier A (W7 position) to D (W3 position).

3.2. The Tilt

The tilt of the spectra was derived by fitting the (X, Y) coordinates of the emission line peaks along the dispersion axis, measured from the negative third to the positive third order (the negative orders at smaller x pixels than the zeroth order x coordinate, the positive ones at larger x pixels). A first order polynomial was used to determine the slope of the spectra with respect the X axis. Repeated measurements were averaged and the standard deviation of the spectra tilt was determined to be typically of $0^{\circ}02$. The average tilt is shown in Table 2 as a function of position in the WFC.

On average, the tilt of the grism spectra in the WFC is $-1^{\circ}98$, and it is field-dependent as it increases along the W7–W3 diagonal by $\simeq 1^{\circ}1$.

Table 2. The X - and Y -shifts and the Spectra Tilt across the WFC Aperture

Position	X -shift (in pixels)	Y -shift (in pixels)	Tilt (in degrees)
W1	113.02	-3.14	-1.91
W2	120.02	-3.56	-1.95
W3	102.02	-1.85	-1.43
W4	106.32	-2.88	-1.85
W5	115.24	-2.77	-1.53
W7			-2.52
W8			-2.11
W9	112.83	-4.57	-2.32
W10	108.15	-3.39	-1.95
Chip1 center	117.32	-4.18	-2.25

3.3. The Separation and Length of the Grism Orders

The distance in pixels of the grism orders from the zeroth order and their approximate length were measured by counting the pixels along the X axis whose counts are 3σ above the background level. The mean length and FWHM of the zeroth order are 23 and 4.4 pixels, respectively. The average (across the f.o.v of the WFC) order separations and lengths are listed in Table 3 in pixels.

Table 3. The Separation from the Zeroth Order and the Length in Pixels of the Grism Orders (from the SMOV data)

Parameter	1 st ord.	2 nd ord.	-1 st ord.	-2 nd ord.
Separation	93	251	-122	-247
Length	156	125	102	111

4. The Method of Wavelength Calibration

The grism spectra were extracted in both units of pixels and wavelength adopting for the latter the wavelength solutions derived from the ground calibrations of the ACS. This allowed us to derive the mean FWHM in Å of the lines in each grism order. The NTT/EMMI template spectra of WR 45 and WR 96 were then convolved by these mean FWHMs, their lines reidentified and the line wavelengths re-measured. The position in pixels of the same lines was measured in the ACS grism spectra with respect to the target X position in the direct image and tables of pixels vs. wavelengths were built. Each table was then fitted with the routine POLYFIT in IRAF and a wavelength solution was determined for each grism order.

This procedure was applied to each grism spectrum in all positions across the f.o.v of the WFC.

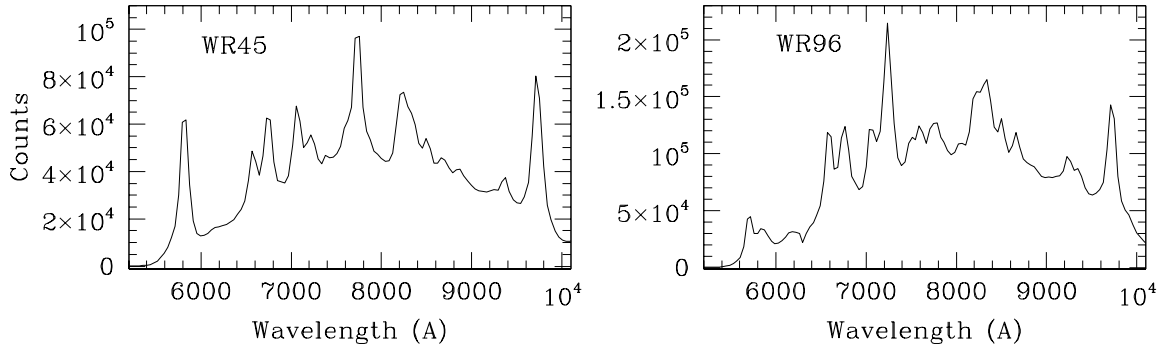


Figure 3. The grism first order spectra acquired for WR 45 at position W1 (left) and WR 96 at the centre of chip 1 (right).

5. The Wavelength Solutions for the WFC and G800L Grism

In this proceeding we present the wavelength solutions (and their field-dependence) computed for the grism first, second and negative first orders which are the brightest. A field map of the dispersion correction for the grism third, negative second and negative third orders can be found in Pasquali et al. (2003).

5.1. The Grism First Order

An example of the grism first order as obtained in position W1 and at the centre of chip 1 is shown in Figure 3 for WR 45 (left) and WR 96 (right).

The dispersion correction for the grism first order is reproduced by a second order polynomial of the form: $\lambda = \lambda_0 + \Delta\lambda_0 X + \Delta\lambda_1 X^2$, where X is the distance along the dispersion axis from the target X position in the direct image.

The wavelength solutions obtained for the ten pointings are reported in Table 4. The tabulated values are averages of multiple measurements of the dispersion parameters derived for each pointing. The typical RMS associated with the fits is 3 Å/pix, while the typical error on λ_0 is 7 Å. The uncertainty in the first-order term of the dispersion ($\Delta\lambda_0$) is 0.2 Å/pix.

Table 4. The Wavelength Solutions Obtained for the Grism First Order as a Function of Position across the f.o.v of the WFC

Position	λ_0 (Å)	$\Delta\lambda_0$ (Å/pix)	$\Delta\lambda_1$ (Å/pix ²)
W1	4815.25	39.79	0.0099
W2	4777.62	37.28	0.0098
W3	4811.80	44.03	0.0096
W4	4760.06	41.94	0.0108
W5	4803.95	39.13	0.0097
W7	4800.86	35.09	0.0068
W8	4772.51	36.23	0.0098
W9	4795.39	39.64	0.0095
W10	4777.90	40.83	0.0130
chip 1 center	4787.27	37.82	0.0112

The first order dispersion ($\Delta\lambda_0$) is clearly field-dependent: it worsens along the diagonal from the W7 (the pointing with the highest dispersion) to the W3 position (lowest

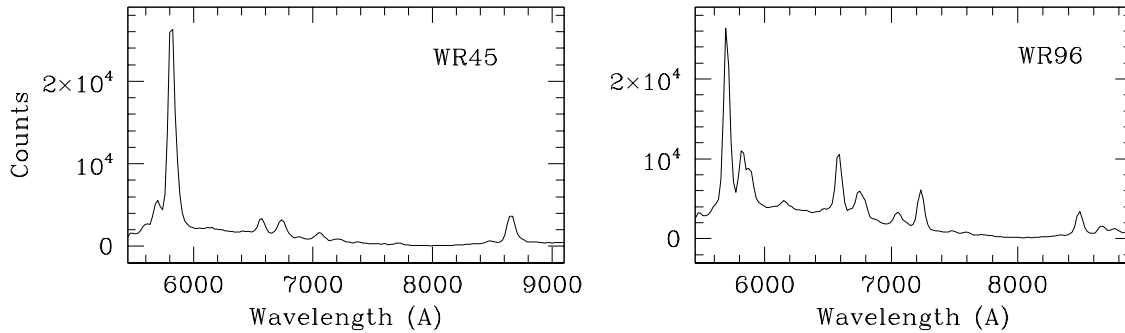


Figure 4. The grism second order spectra acquired for WR 45 at position W1 (left) and WR 96 at the centre of chip 1 (right).

dispersion) by 22% of the value at position W1. Alternatively, it can be said that the amplitude of the field-dependence between the centre of chip 2 and the W3 and W7 corners is 11% of the value in the W1 position.

5.2. The Grism Second Order

The grism second order spectra obtained in the W1 position and at the centre of chip 1 are plotted in Figure 4 for both WR 45 and WR 96.

The second order overlaps with the first order at $\lambda \simeq 5400 \text{ \AA}$ and does not extend beyond 9000 \AA . For these reasons, the wavelength solution was determined with a first-order polynomial fit, i.e., $\lambda = \lambda_0 + \Delta\lambda_0 X$, where X is again the distance along the dispersion axis from the target X position in the direct image.

The results are listed in Table 5. As for Table 4, these values are averages among multiple measurements available at each pointing. Typical standard deviations are 0.1 \AA/pix and 7 \AA on the dispersion and zero point, respectively. The RMS values of the fits are about 3 \AA .

Table 5. The Wavelength Solutions Obtained for the Grism Second Order as a Function of Position across the f.o.v of the WFC.

Position	λ_0 (\AA)	$\Delta\lambda_0$ (\AA/pix)
W1	2432.38	20.75
W2	2400.40	19.63
W3	2445.01	22.85
W4	2411.01	21.89
W5	2405.74	20.54
W7	2411.48	18.33
W8	2391.95	19.13
W9	2418.70	20.72
W10	2409.33	21.56
chip 1 center	2406.73	19.98

The field dependence noticed earlier for the grism first order is also present in the dispersion of the second. The amplitude of the dispersion variation from center to the W7 and W3 corners is about 11% of the dispersion in the W1 position. Once again, the dispersion decreases along the diagonal from W7 to W3.

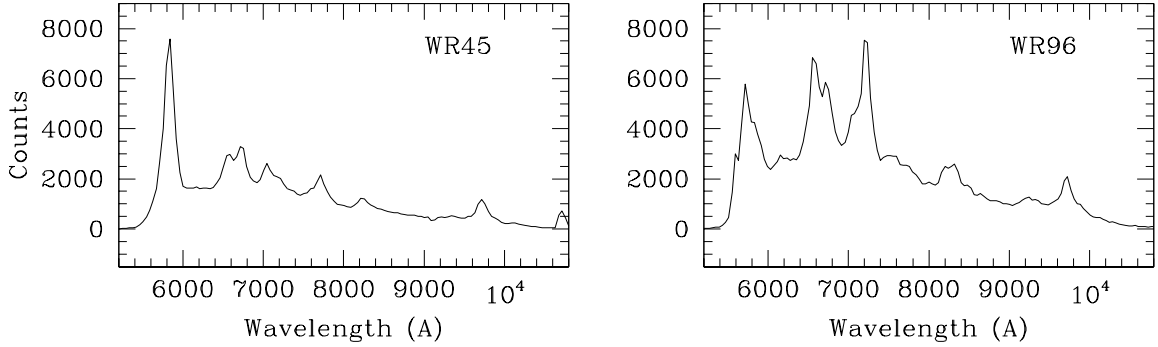


Figure 5. The grism negative first order spectra acquired for WR 45 at position W1 (left) and WR 96 at the centre of chip 1 (right).

5.3. The Grism Negative First Order

The negative first order spectra of WR 45 and WR 96 are shown in Figure 5.

Since the resolution is here lower than for the positive first order and the noise higher, the wavelength solution of the negative first order was fitted with a first-order polynomial, $\lambda = \lambda_0 + \Delta\lambda_0 X$ where X is the distance in pixels along the dispersion axis from the target X position in the direct image. The measurements of dispersion and zero point obtained from multiple spectra acquired at the same pointing were averaged and are presented in Table 6.

Table 6. The Wavelength Solutions Obtained for the Grism Negative First Order as a Function of Position across the f.o.v of the WFC.

Position	λ_0 (Å)	$\Delta\lambda_0$ (Å/pix)
W1	-4820.51	-41.71
W2	-5026.08	-40.05
W3	-4882.90	-46.48
W4	-4808.92	-44.37
W5	-4995.32	-41.54
W7		
W8		
W9	-4858.67	-41.96
W10	-4862.51	-43.81
chip 1 center	-4784.49	-40.14

Since W7 and W8 positions are closer to the edge of the field than W5 (cf. Figure 2), the negative first order falls physically outside the frame. Nevertheless, a variation in the dispersion of about 11% of the value in W1 is still detected between the W1 and W3 positions. The standard deviation is 0.1 Å/pix and 27 Å on the dispersion and the zero point, respectively. The typical RMS of the first-order polynomial fits is 9 Å.

6. Products Delivered to Users

The average dispersion coefficients derived for the ten positions across the f.o.v of the WFC have to be parametrized as a function of position in order to extract and calibrate

spectra anywhere within the WFC aperture. We thus derived a two dimensional fit for each parameter of the dispersion solutions of each grism order, where each parameter is a function of the (X, Y) coordinates of the target in the direct image. These 2D fits were performed by adopting surface fits polynomials. The same was also done for the X - and Y -shifts, the tilt of the spectra, the orders separation and length.

The above fits are stored in calibration files used by the ST-ECF slitless spectra extraction code aXe (Pirzkal et al. 2001a) and are delivered together with the software package.

Once the wavelength solution was determined, the flat-field correction and the flux calibration using the SMOV and INTERIM spectra of two white dwarfs, GD 153 and G191B2B could be formalised. This is fully described in Pirzkal et al., this volume, p. 74. It is also possible, at this stage of the calibrations, to correct the extracted spectra for CCD fringing. The modeling of the WFC fringing is explained in detail in Walsh et al., this volume, p. 90.

References

- van der Hucht, K. A. 2001, *The VIIth Catalogue of Galactic Wolf-Rayet Stars*, New AR, 45, 135
- Pasquali, A., Pirzkal, N., & Walsh, J. R. 2001a, *Selection of Wavelength Calibration Targets for the ACS Grism*, ST-ECF Instrument Science Report ACS 2001-04
- Pasquali, A., Pirzkal, N., & Walsh, J. R. 2003, *The In-orbit Wavelength Calibration of the WFC Grism*, ST-ECF Instrument Science Report ACS 2003-01, in preparation
- Pasquali, A., Pirzkal, N., Walsh, J. R., Hook, R. N., Freudling, W., Albrecht, R., Fosbury, R. A. E. 2001b, *The Effective Spectral Resolution of the WFC and HRC Grism*, ST-ECF Instrument Science Report ACS 2001-02
- Pirzkal, N., Pasquali, A., & Demleitner, M. 2001a, ST-ECF Newsletter, 29, 5
- Pirzkal, N., Pasquali, A., Walsh, J. R., Hook, R. N., Freudling, W., Albrecht, R., & Fosbury, R. A. E. 2001b, *ACS Grism Simulations using SLIM 1.0*, ST-ECF Instrument Science Report ACS 2001-01